Characterizing Ballast Degradation Through Los Angeles Abrasion Test and Image Analysis

Yu Qian, Huseyin Boler, Maziar Moaveni, Erol Tutumluer, Youssef M. A. Hashash, and Jamshid Ghaboussi

Ballast fouling, often associated with deteriorating railroad track performance, refers to the condition in which the ballast layer changes its composition and develops a much finer grain size distribution. Fouling is commonly caused by degradation or breakage of ballast aggregates under traffic loading, although other fine materials including but not limited to coal dust, fine-grained subgrade soils, and sand can also contaminate a clean and uniformly graded ballast layer. An experimental approach is described to characterize stages of railroad ballast degradation studied through Los Angeles abrasion testing in the laboratory. An aggregate image analysis approach is used to investigate ballast particle abrasion and breakage trends at every stage through detailed quantifications of individual ballast particle size and shape properties. The experimental study indicated that the fouling index (FI) commonly used by practitioners was indeed a good indicator of fouling conditions, especially when all voids created by larger particles were filled by fine materials as FI values approached 40. Image analysis results of ballast particles larger than 9.5 mm (⅜ in.) scanned after a number of turns of the Los Angeles abrasion drum showed good correlations between percentage changes in aggregate shape properties, that is, imaging-based flatness and elongation, angularity and surface texture indexes, and the FI. The establishment of such relationships between in-service track fouling levels and ballast size and shape properties with similar field imaging techniques would help to understand field degradation trends better and as a result improve ballast serviceability and life-cycle performance.

Railroad ballast is uniformly graded coarse aggregate placed between and immediately underneath the crossties. The purpose of ballast is to provide drainage and structural support for the loading applied by trains. As ballast ages, it is progressively fouled with materials finer than aggregate particles. Fouling refers to the condition of railroad ballast when voids in this unbound aggregate layer are filled with relatively finer materials or fouling agents commonly from the ballast aggregate breakdown and outside contamination (e.g., coal dust from coal trains or subgrade soil intrusion). Often associated with railroad track performance concerns, such as poor drainage, rapid and excessive settlement, and reduced lateral stability, ballast fouling and degradation are considered unfavorable and are routinely addressed through ballast cleaning, undercutting, and other track maintenance activities.

Department of Civil and Environmental Engineering, University of Illinois at Urbana–Champaign, 205 North Mathews, Urbana, IL 61801. Corresponding author: E. Tutumluer, tutumlue@illinois.edu.

Transportation Research Record: Journal of the Transportation Research Board, No. 2448, Transportation Research Board of the National Academies, Washington, D.C., 2014, pp. 142–151.
DOI: 10.3141/2448-17

Previous research studies reported that the main cause of ballast fouling was the degradation and breakdown of the uniformly graded large ballast particles under repeated traffic loading (*1, 2*). Selig and Waters concluded that up to 76% of the ballast fouling was due to ballast breakdown, in other words, ballast degradation (*3*). Accordingly, to quantify ballast fouling conditions, Selig and Waters proposed two indexes: the fouling index (FI) and the percentage of fouling. Simply, FI is the summation of the percentage by weight of ballast material passing the 4.75-mm (No. 4) sieve and the percentage passing the 0.075-mm (No. 200) sieve. Percentage of fouling is the ratio of the dry weight of material passing the 9.5-mm (⅜-in.) sieve to the dry weight of the total sample. In the context of this study, fines are those materials with particle sizes less than 9.5 mm or passing the ⅜-in. sieve.

Increased ballast settlements were reported by researchers when the amount of fouling material in ballast increased (*4*–*6*). Raymond and Diyaljee also observed more severe wear of the tie at heavily fouled track locations caused by the reduced load-bearing ability of the track (*6*). Huang et al. conducted a series of shear strength tests with a large-scale direct shear box apparatus to investigate ballast behavior when different fouling materials (e.g., clay, mineral filler, and coal dust) were mixed with clean ballast at different weight percentages (*7*). Numerical simulations of the ballast shear box tests were also performed through the use of the discrete element method (DEM) (*8*). From that study, coal dust was highlighted as the most detrimental fouling agent. Similarly, Indraratna et al. performed drained triaxial tests to study clay-fouled ballast behavior since soft subgrade soil pumping and intrusion have become the recent focus in Australia (*9*). Although proper consideration needs to be given to better understand the effects of such outside fouling agents, a large portion of the annual operating budget to sustain the railway track system goes toward the maintenance and renewal of fouled ballast that is fouled because of ballast breakdown or degradation instead of contamination by outside fouling agents (*3*).

Several laboratory tests were proposed in previous studies to generate fouled ballast from ballast degradation, such as the Los Angeles (LA) abrasion test, mill abrasion test, Deval abrasion test, and micro-Deval abrasion test. Lim (*10*) and McDowell et al. (*11*) found the LA abrasion test results to correlate well with ballast box test results when tamping was included in their experiments; this finding was also confirmed by Aursudkij (*12*). Both toughness and hardness are important properties of aggregates. Although the

former is a measure of resistance to breakage, the latter is more related to durability of the wearing surface. Commonly, LA abrasion tests are believed to measure aggregate toughness, not hardness. Use of only the LA abrasion value may not be sufficient to predict ballast aggregate degradation characteristics in the field (*6*). Raymond and Diyaljee suggested additional tests to measure the hardness of aggregates, such as the mill abrasion test (*6*). Unlike the LA abrasion test, mill abrasion tests tended to create finer material passing the 0.075-mm sieve since degradation was mostly caused by wearing aggregates (*13*). Klassen et al. introduced the abrasion number as the sum of LA abrasion and five times the mill abrasion values (*14*). Raymond and Bathurst stated that the abrasion number had good correlation with ballast permanent deformation characteristics from cyclic triaxial testing (*15*).

Traditional abrasion tests such as Deval abrasion or LA abrasion do not include any moisture. To investigate moisture effects on aggregate degradation, the micro-Deval abrasion test was created in France during the 1960s. Similar to the mill abrasion test, no impact load is involved in this test, and abrasion is caused by aggregates' wearing of each other (*16*). Fowler et al. reported that the micro-Deval abrasion test adequately predicted aggregate field performance in flexible and rigid pavements, and no improved predictions were obtained when micro-Deval abrasion test results were combined with those from LA abrasion tests (*17*). Recent findings on the degradation trends of Norwegian ballast materials evaluated from triaxial testing concluded that LA abrasion test results correlated with the actual material breakdown better than micro-Deval abrasion test results (*18*).

To improve the understanding of ballast performance associated with its usage and life-cycle degradation due to particle abrasion and breakage, both ballast particle size and shape properties at different fouling conditions, which typically change according to the service tonnage of the track in the field, need to be systemically evaluated. Preliminary results are presented of an ongoing comprehensive research study at the University of Illinois with the goal to characterize ballast degradation through LA abrasion testing and aggregate image analysis. A series of LA abrasion tests performed to continuously break down a commonly used granite-type ballast specimen revealed quite important linkages between ballast fouling and degradation trends quantified by imaging-based changes in particle size and shape properties.

OBJECTIVE AND SCOPE

The overall objective of the ongoing research at the University of Illinois is to develop the ballast DEM modeling capability as a quantitative track performance simulation tool to better understand (*a*) the nature of ballast particulate interactions through strength, modulus, and deformation testing; (*b*) complex ballast behavior under dynamic train loading regimes in the field; and (*c*) fouling and degradation trends and their impact on track performance. This study has a research scope primarily focused on characterizing ballast degradation by using LA abrasion tests, which can generate fouled ballast through accelerating ballast degradation, and the aggregate image analysis approach. Imaging-based quantifications of changes in sizes and shapes of individual particles in a test specimen can identify degradation trends of certain ballast material in a controlled laboratory environment. The laboratory findings should always be linked to field degradation and ballast fouling conditions through similar image analysis techniques currently applied in the field for ballast serviceability and performance monitoring.

EXPERIMENTAL STUDY WITH LA ABRASION TEST

Ballast Material, Test Device, and Test Procedure

The ballast material used in the laboratory was a 100% crushed granite, which adequately met the American Railway Engineering and Maintenance-of-Way Association (AREMA) No. 24 gradation requirements as shown in Figure 1. Ten kilograms of new ballast material was placed in the LA abrasion drum together with 12 steel balls (Figure 2). The drum was set to rotate on average 50 turns per minute and for each run the drum rotated 250 times. After finishing 250 turns, the drum was allowed to stand still for 10 min to let the dust settle before the tested material was poured out. In order to minimize the loss of fine materials, both the inside of the drum and the steel balls were carefully hand brushed after every 250 turns. All particles more than 25.4 mm or passing the 1.0-in. sieve were also brushed to collect dust and fine material before sieving. The rest of the materials (passing 25.4 mm) were carefully sieved by using

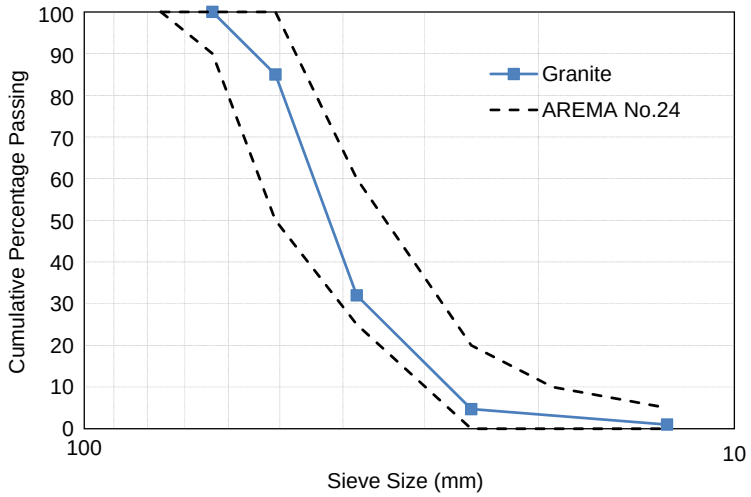

FIGURE 1 Gradation properties of granite ballast material.

(a) **(b)** **(c)** **(d)**

FIGURE 2 LA abrasion test equipment and specimen: (*a*) LA abrasion test device, (*b*) ballast and steel balls before test, (*c*) ballast and steel balls after test, and (*d*) brushing large particles before sieving.

a DuraShake rotation aggregate sifter to minimize the loss of fine materials.

Materials passing each sieve size were then collected and placed on a blue tarp and photographs were taken. In addition, aggregate particles larger than 9.5 mm or passing the 3/8-in. sieve were hand collected to conduct image analysis with the enhanced University of Illinois aggregate image analyzer (E-UIAIA) (*19*). This step was conducted to determine imaging-based quantifications of particle size and shape indexes after every 250 turns before all materials were mixed together for the next LA abrasion run. The outlined procedure was repeated until the specimen reached a Selig and Waters FI of 40 (*3*), which corresponds to a heavily fouled ballast condition requiring maintenance activities on the track. The same specimen was always used during the LA abrasion testing, which required eight individual runs at 250-turn intervals. In order to reach an FI of 40, an additional 125 turns of the drum were also needed to complete the test at 2,125 drum turns.

Test Results

Figure 3 shows the gradation curves obtained from the sieve analysis test results of the granite specimen after the total 2,125 turns of the LA abrasion drum. By carefully preparing and handling the same specimen through the nine intermediate steps of the LA abrasion runs and sieve analyses, only 160 g of material was lost, 1.6% of the total initial weight. Figure 3 also presents the FI values calculated for each gradation curve. With the number of turns increasing in the LA abrasion test, the ballast specimen changed gradually from uniformly graded to more well graded. This change is also indicated by the increasing FI values with a decreasing rate (Figure 3). No doubt clean ballast material was more susceptible to abrading sharp corners and edges of the crushed particles. Breakage of the large-sized particles mostly happened in the early stages of the experiment as well. With the number of turns increasing in the LA abrasion runs, those particles that did not break because of the impact loads eventually became more rounded because of chipping corners and smoother textures from the abrasion of surfaces and edges.

The overall particle size degradation trends and the changes in proportion to the original particle sizes are visualized in Figure 4 for up to 2,125 LA abrasion drum turns. For the first 250 turns, the specimen degraded from the original clean ballast with a particle size distribution that had an FI value of 0 to a fouled ballast condition with an FI value of 7. The initial abrasion and breakage of the large particles immediately created both smaller particles and fine materials, that is, particles less than 9.5 mm or passing the ⅜-in. sieve, as shown

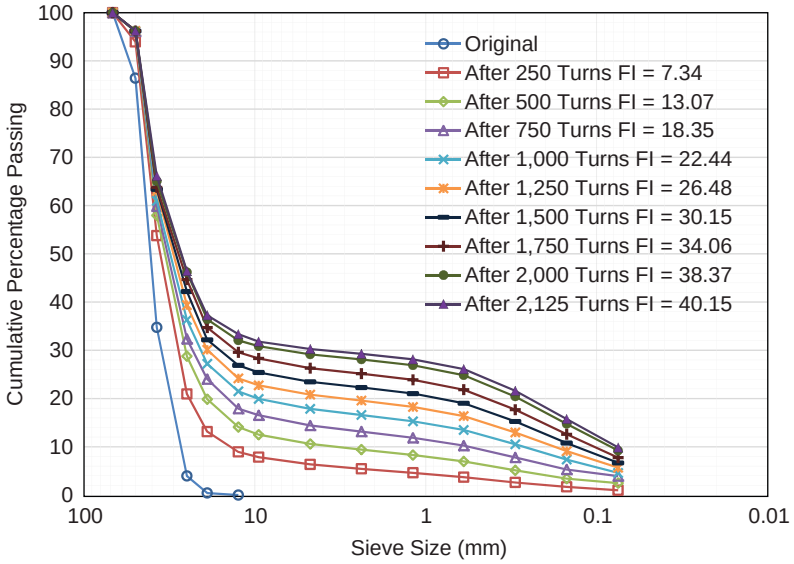

FIGURE 3 Gradations of granite ballast changing with LA abrasion drum turns.

No. of turns \ Opening size	50 mm	37.5 mm	25.0 mm	19.0 mm	12.5 mm	9.5 mm	4.75 mm	2.36 mm	1.18 mm	0.60 mm	0.30 mm	0.15 mm	0.075 mm	Pan
0														
No. of particles	7	37	64	19	8									
250														
No. of particles	3	29	65	44	65	51								
500														
No. of particles	2	28	58	48	94	70								
750														
No. of particles	2	28	58	46	102	66								
1,000														
No. of particles	2	28	51	50	94	72								
1,250														
No. of particles	2	27	49	49	90	69								
1,500														
No. of particles	2	27	43	52	82	70								
1,750														
No. of particles	2	27	37	52	77	57								
2,000														
No. of particles	2	26	35	53	65	58								
2,125														
No. of particles	2	25	37	49	55	67								

FIGURE 4 Particle size degradation trends with LA abrasion drum turns (no. = number).

in Figure 4. For example, in the case of the original clean ballast specimen, 7 particles were retained on the 50-mm sieve and 37 particles were retained on the 37.5-mm sieve. After the 2,125 LA abrasion drum turns, these particle counts decreased to 2 and 25 for particles retained on the 50-mm and 37.5-mm sieves, respectively.

For some sieve sizes (e.g., 12.5 mm) the number of particles generated throughout the experiment increased first and decreased later. In this case, additional particles were created first when the larger sizes were broken down, and then these 12.5-mm particles were broken into smaller sizes when the number of drum turns further increased. As discussed earlier, at the later stages of the experiment, the FI increased with a decreasing rate, which implied that particles became not only smaller but also smoother and more rounded, thus becoming more resistant to abrasion and breakage. For example, Figure 4 provides visual evidence about how those particles retained on the 37.5-mm sieve indeed became smoother and rounded after 500 turns. However, the number of particles retained on the 37.5-mm sieve did not change significantly because those particles did not break and no new particles were created from larger particle degradation (e.g., particles retained on the 50-mm sieve) (see Figure 4). More detailed analyses of the degradation trends including particle shape indexes quantified from the image analysis approach will be discussed later and these findings will be confirmed.

Gradation curves and visualizations of individual particle sizes at different LA abrasion turns indeed provide valuable information for the ballast aggregate composition at different fouling levels. However, it is not obvious how to relate these degradation trends to ballast layer functional characteristics and governing mechanisms that would affect field ballast layer structural and drainage behavior. A better understanding could be gained by understanding several important concepts: how material would pack, how much void space would be available for drainage, and whether there would be individually contacting larger particles (i.e., a load-carrying aggregate skeleton) left in the ballast layer associated with different levels of fouling. In order to investigate particle contact and particle packing characteristics, the test specimen collected after every 250 turns of the LA abrasion test was poured into an acrylic chamber with dimensions of 25.4 cm (10.0 in.) in diameter and 25.4 cm (10.0 in.) in height. Figure 5 presents the side and top views of aggregate packing photographs taken at different numbers of LA abrasion drum turns with the corresponding FI values. Because of the continuous abrasion and breakage of particles throughout the test, the total height of the test specimen decreased substantially. After 2,125 turns the void space remaining among particles is visualized in Figure 5. The fine materials accumulate from the bottom to fill all the voids created by the fewer large particles at the top as the FI approaches 40. This finding is in good agreement with what was suggested by Selig and Waters as the limit of fouled ballast that should no longer be used in the field (*3*).

AGGREGATE IMAGE ANALYSIS

Image Analysis and E-UIAIA

Besides the grain size distribution, ballast aggregate morphological or shape properties, especially the flatness and elongation ratio, the angularity index, and the surface texture index, are key indexes quantified by the UIAIA (*19*). Figure 6 shows the recently enhanced aggregate image analyzer (E-UIAIA) with three high-resolution color cameras for taking three orthogonal views of a scanned aggregate particle to determine its particle shape indexes. Such an approach to quantify individual particle shapes and re-create polyhedron elements of crushed stone materials has already been successfully utilized in the ballast DEM model simulations (*20–26*). In this study, the image analysis approach adopted could adequately quantify changes in shape indexes of individual particles utilized in the LA abrasion test specimen (*27*). After each 250 turns, all the particles larger than 9.5 mm (⅜ in.) were collected to conduct image analyses so that certain trends in ballast particle shape degradation could be identified and linked to FI values.

Image Analysis Results

Table 1 gives all the averaged values of the flatness and elongation ratio, angularity index, and the surface texture index determined for particles retained on different sieve sizes above 9.5 mm (⅜ in.) after different numbers of turns. Two trends are observed:

1. For a certain particle size, the shape properties, angularity index, and surface texture index commonly decrease as the number of drum turns increases (see individual rows from left to right in Table 1), which confirms through quantitative imaging-based indexes that the same particles tend to be smoother and more rounded during LA abrasion testing; and
2. For a certain number of drum turns, the angularity index and surface texture index generally increase as particle size decreases (see individual columns from top to bottom in Table 1). That is, smaller particles created from the breakage of larger particles initially have more crushed faces and thus they are more angular and rougher textured when compared with the larger particles that often experience abrasion only.

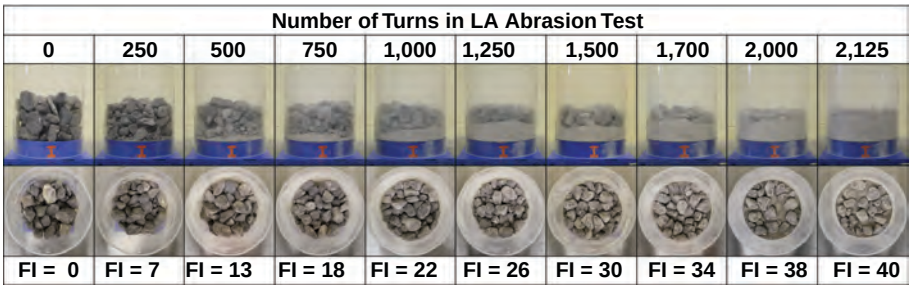

FIGURE 5 Side and top views of plexiglas cylinder showing particle packing.

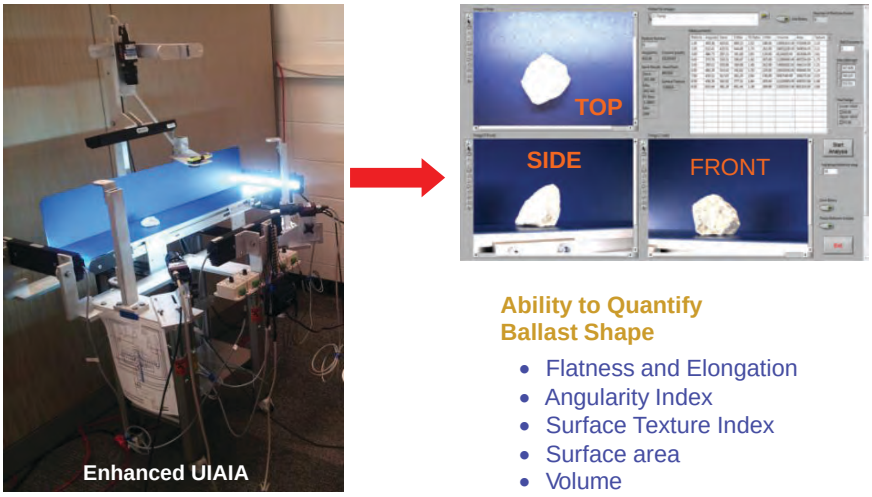

FIGURE 6 Image analysis approach with E-UIAIA.

Also, in Table 1 the total number of particles above 9.5 mm (⅜ in.) initially increased from 135 to 302 rapidly and then decreased to 235 as FI values increased to 40. This finding also quantitatively explained that the large particles were more likely to break in the beginning and, thus, created smaller particles quickly but tended to become more resistant to abrasion and breakage later on. A recent field imaging study successfully detected the gradual decrease in the aggregate size and changes of particle shape properties with increased ballast depth; those findings agreed with the findings in this study (*28*).

Figures 7 through 9 present the distributions of the shape indexes, the angularity index, the surface texture index, and the flatness and elongation ratio for the particles scanned by the E-UIAIA. Each value of an imaging-based shape index was determined from scanning a particle after every 250 turns of the LA abrasion equipment and sorting according to magnitude for plotting with the cumulative

TABLE 1 Properties and E-UIAIA–Based Shape Indexes of Ballast Specimens Tested

	Number of Turns									
Opening Size (mm)	0	250	500	750	1,000	1,250	1,500	1,750	2,000	2,125
Angularity index										
50	388	326	301	280	222	245	213	199	214	224
37.5	377	295	299	272	258	243	230	226	208	211
25.0	384	337	310	292	274	262	254	253	248	241
19.0	416	337	312	310	292	281	274	274	274	267
12.5	441	367	354	346	338	321	322	312	309	312
9.5	—	383	378	356	363	351	350	370	364	369
Average	401	341	326	309	291	284	274	274	269	271
Flatness and elongation ratio										
50	2.2	2.0	1.9	2.0	2.0	2.0	1.9	1.9	1.9	1.9
37.5	2.3	2.0	1.9	1.9	1.8	1.9	1.8	1.8	1.8	1.8
25.0	2.2	2.0	2.0	1.9	1.8	1.9	1.8	1.8	1.7	1.7
19.0	2.4	2.1	1.9	1.8	1.8	1.7	1.8	1.8	1.8	1.8
12.5	2.4	2.0	1.9	1.9	1.8	1.8	1.8	1.7	1.7	1.7
9.5	—	2.1	2.0	1.9	1.8	1.8	1.8	1.8	1.8	1.8
Average	2.3	2.0	1.9	1.9	1.8	1.8	1.8	1.8	1.8	1.8
Surface texture index										
50	1.3	0.9	0.9	0.8	0.9	0.9	0.9	0.7	0.7	0.6
37.5	1.3	1.0	0.9	0.9	0.8	0.8	0.8	0.8	0.8	0.8
25.0	1.4	1.2	1.1	1.0	0.9	0.9	0.8	0.9	0.9	0.9
19.0	1.6	1.3	1.1	1.1	1.1	1.0	1.1	1.1	1.0	1.0
12.5	2.0	1.5	1.3	1.3	1.3	1.2	1.2	1.2	1.0	1.0
9.5	—	1.7	1.5	1.4	1.5	1.4	1.4	1.4	1.4	1.4
Average	1.5	1.3	1.1	1.1	1.1	1.0	1.0	1.0	1.0	1.0
Total number of particles	135	257	300	302	297	286	277	253	239	235

NOTE: na = not applicable.

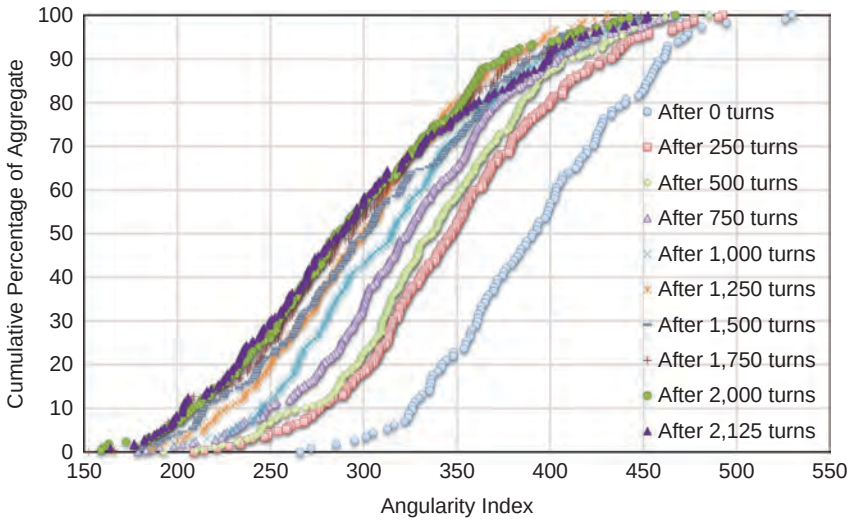

FIGURE 7 Angularity index distribution trends after LA abrasion drum turns.

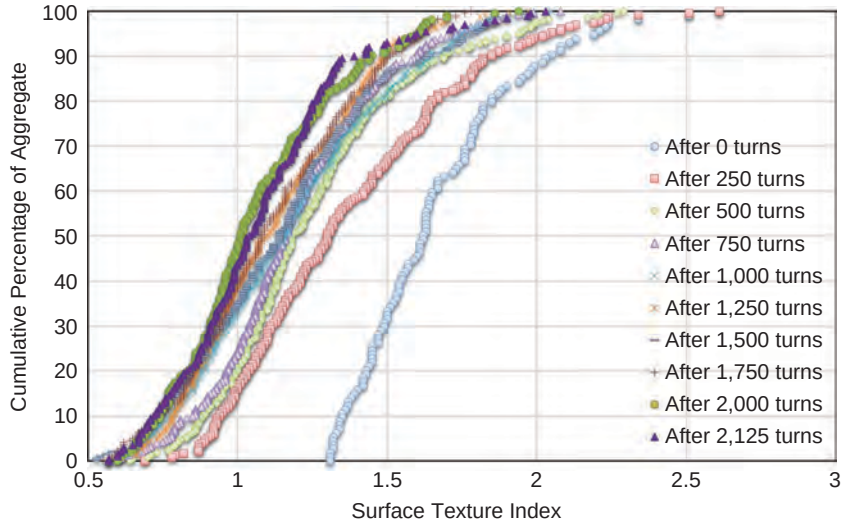

FIGURE 8 Surface texture index distribution trends after LA abrasion drum turns.

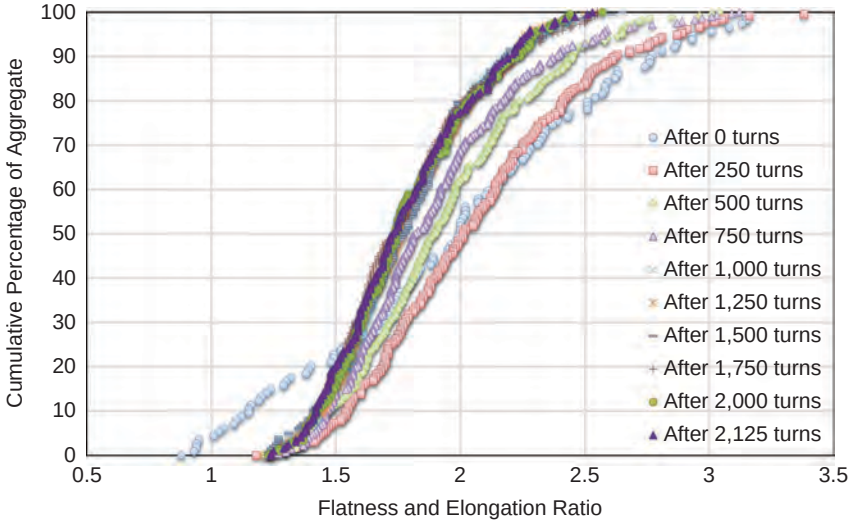

FIGURE 9 Flatness and elongation ratio distribution trends after LA abrasion drum turns.

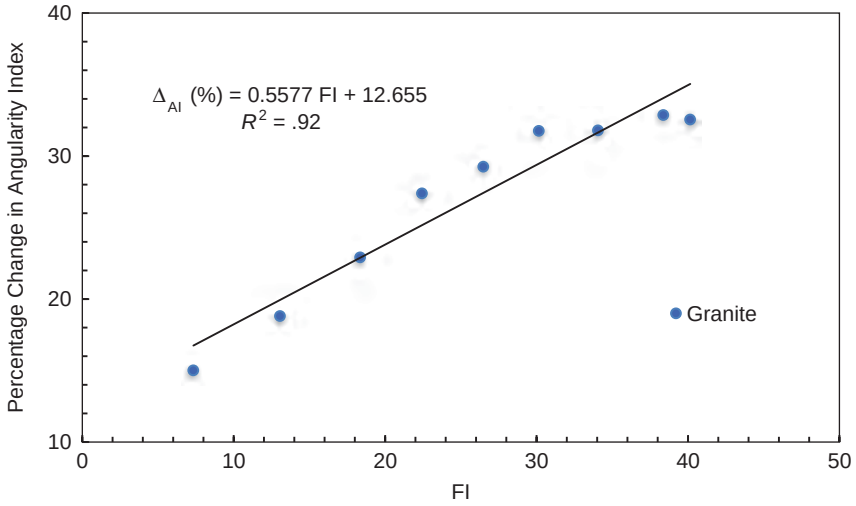

FIGURE 10 Percentage change in angularity index (AI) correlated with FI.

number of aggregate particles passing as a percentile value. Similar to the grain size distribution concept, Figures 7 through 9 present the overall degradation trends of a certain aggregate shape property with the increasing number of LA abrasion drum turns. Accordingly, Figure 7 shows angularity index distributions in which each point represents the angularity index value for a particle and each curve captures the angularity index distribution for all the particles after a certain number of drum turns. The gap between any two curves implies how much the angularity index changed between the different numbers of turns. Clearly, the angularity index decreases at a slower rate when moving away from the original curve. Accordingly, the distribution curves tend to get closer to each other as they shift toward the left, which represents a higher number of drum turns. Similarly, Figure 8 shows the surface texture index distributions and similar patterns are observed. Further, Figure 9 presents the flatness and elongation ratio distributions in the same manner. Differing from the angularity index and surface texture index trends, the flatness and elongation ratio distributions change from the initial wider-range values to much narrower-range values. This finding means that particles generally tend to converge to a certain shape and often become more cubical when most of the originally flat and elongated particles are degraded because of abrasion and breakage.

As clearly seen in Figure 5, the FI of Selig and Waters is a good indicator of the ballast fouling condition as it relates to reduced void space and increased particle packing in this well-graded and smaller top–sized fouled ballast layer composition (*3*). Because both ballast fouling and shape property changes are due to particle abrasion and breakage from LA abrasion drum turns, the next step was to investigate how the change in FI values would correlate with changes in aggregate particle shape indexes quantified by the E-UIAIA. Indeed, Figure 10 shows a strong correlation between the percentage change in average angularity index values and the FI with a coefficient of determination (R^2) of 92%. Similarly, Figure 11 presents another strong correlation between the percentage change in average surface

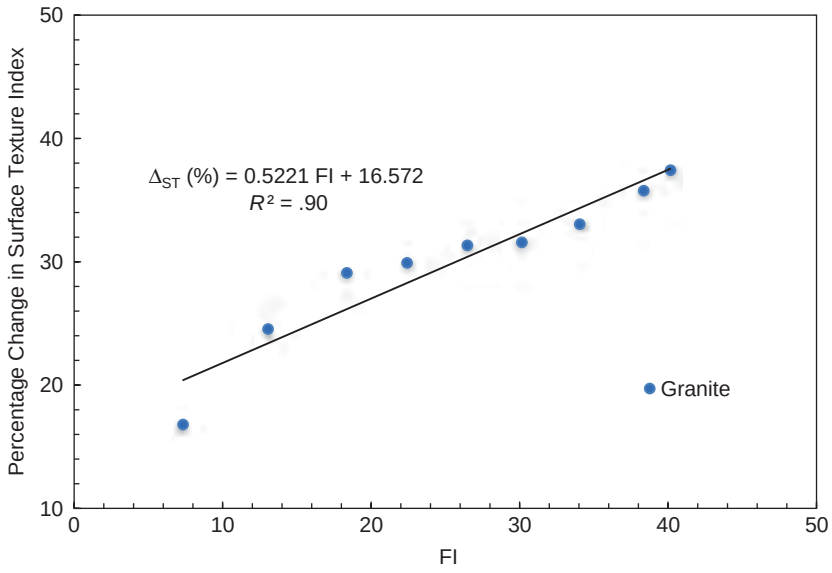

FIGURE 11 Percentage change in surface texture (ST) index correlated with FI.

texture indexes and the FI, this time with a coefficient of determination (R^2) of 90%. Such trends as those shown in Figures 10 and 11 suggest that there is a definite correlation between ballast fouling and the overall reduced angularity and surface texture properties of ballast aggregate particles; this finding was also highlighted recently from field degradation trends by Moaveni et al. (*28*).

Accordingly, such relationships found between ballast fouling levels and degradation in ballast size and shape properties could help to improve DEM ballast modeling efforts by simulating realistically ballast behavior at different fouling levels and utilizing field imaging techniques to determine field ballast serviceability. There is certainly more to learn by linking these findings with field degradation trends to capture both spatial property variability and property changes within the ballast layer depth to establish field usage and ballast life cycle under revenue service loading.

CONCLUSIONS

A detailed experimental study is presented focused on characterizing ballast aggregate degradation by using LA abrasion tests, which can generate fouled ballast through accelerating ballast degradation, and an aggregate image analysis approach. An LA abrasion test specimen of commonly used granite-type ballast material was monitored for degradation and fouling trends with the help of imaging-based quantifications of changes in sizes and shapes of individual particles in a controlled laboratory environment. Detailed grain size distributions, void space and particle packing, and particle shape properties were analyzed. The following conclusions can be drawn from this study:

1. The LA abrasion test in a laboratory environment generates fouled ballast materials through abrasion and breakage of large particles, thus creating smaller particles and fine materials. This research provided visual evidence to show that fouling materials accumulate starting from the bottom of the ballast layer and gradually fill the voids created by particles larger than 9.5 mm (⅜ in.).
2. The FI, a summation of the percentage by weight of ballast samples passing the 4.75-mm (No. 4) sieve and the percentage passing the 0.075-mm (No. 200) sieve, is a good indicator of ballast fouling conditions. When the FI approached 40, nearly all voids among the larger particles were filled with finer materials from ballast degradation.
3. Image analyses of particles larger than 9.5 mm presented clear trends of changes in both particle size and shape (i.e., flatness and elongation, angularity, and surface texture) properties. As the FI increased, the particles became smoother and more rounded and thus more resistant to abrasion and breakage.
4. There is a clear relationship between the FI and the overall shape reductions in angularity and surface texture properties of the aggregate particles larger than 9.5 mm. Ballast degradation trends to be monitored in the field with imaging techniques will potentially provide field-validated relationships between ballast fouling levels and ballast size and shape properties that could help to improve ballast DEM modeling efforts and adequately establish field ballast serviceability and maintenance needs and life-cycle performance.

ACKNOWLEDGMENTS

This research project was partially supported by the FRA. Wenting Hou of the Department of Civil and Environmental Engineering at the University of Illinois at Urbana–Champaign, provided considerable help with the laboratory image analyses. The support and help are greatly appreciated.

REFERENCES

1. Selig, E. T., B. I. Collingwood, and S. W. Field. Causes of Fouling in Track. *AREA Bulletin 717*, 1988.
2. Selig, E. T., V. DelloRusso, and K. J. Laine. *Sources and Causes of Ballast Fouling.* Report R-805. Association of American Railroads, Technical Center, Chicago, Ill., 1992.
3. Selig, E. T., and J. M. Waters. *Track Geotechnology and Substructure Management.* Thomas Telford Publications, London, 1994.
4. Chiang, C. C. *Effects of Water and Fines on Ballast Performance in Box Tests.* MS Project Report AAR89-366P. University of Massachusetts, Amhurst, 1989.
5. Han, X., and E. T. Selig. Effects of Fouling on Ballast Settlement. *Proc., 6th International Heavy Haul Railway Conference,* Cape Town, South Africa, 1997.
6. Raymond, G. P., and V. Diyaljee. Railroad Ballast Load Ranking Classification. *Journal of the Geotechnical Engineering Division,* ASCE, Vol. 105, No. 10, 1979, pp. 1133–1153.
7. Huang, H., E. Tutumluer, and W. Dombrow. Laboratory Characterization of Fouled Railroad Ballast Behavior. In *Transportation Research Record: Journal of the Transportation Research Board, No. 2117,* Transportation Research Board of the National Academies, Washington, D.C., 2009, pp. 93–101.
8. Huang, H., and E. Tutumluer. Discrete Element Modeling for Fouled Railroad Ballast. *Construction and Building Materials,* Vol. 25, 2011, pp. 3306–3312.
9. Indraratna, B., N. Tennakoon, S. Nimbalkar, and C. Rujikiatkamjorn. Behavior of Clay-Fouled Ballast Under Drained Triaxial Testing. *Géotechnique,* Vol. 63, No. 5, 2012, pp. 410–419.
10. Lim, W. *Mechanics of Railway Ballast Behavior.* PhD dissertation. University of Nottingham, United Kingdom, 2004.
11. McDowell, G., W. Lim, A. Collop, R. Armitage, and N. Thom. Laboratory Simulation of Train Loading and Tamping on Ballast. *Proceedings of the Institution of Civil Engineers–Transport,* Vol. 158, No. 2, 2005, pp. 89–95.
12. Aursudkij, B. *A Laboratory Study of Railway Ballast Behavior Under Traffic Loading and Tamping Maintenance.* PhD dissertation. University of Nottingham, United Kingdom, 2007.
13. Selig, E., and D. Boucher. Abrasion Tests for Railroad Ballast. *ASTM Geotechnical Testing Journal,* Vol. 13, No. 4, 1990, pp. 301–311.
14. Klassen, M. J., A. W. Clifton, and B. R. Watters. Track Evaluation and Ballast Performance Specifications. In *Transportation Research Record 1131,* TRB, National Research Council, Washington, D.C., 1987, pp. 35–44.
15. Raymond, G., and R. Bathurst. Repeated Load Response of Aggregates in Relation to Track Quality Index. *Canadian Geotechnical Journal,* Vol. 31, No. 4, 1994, pp. 547–554.
16. Williams, G., K. Hampel, J. Allen, and D. Fowler. Update on ICAR 507: The Significance and Application of the Micro-Deval Test. *Proc., International Center for Aggregate Research 13th Annual Symposium,* April 10–13, Austin, Tex., 2005.
17. Fowler, D., J. Allen, A. Lange, and P. Range. *The Prediction of Coarse Aggregate Performance by Micro-Deval and Other Aggregate Tests.* Technical Report ICAR 507-1F. Aggregate Foundation for Technology, Research, and Education, Alexandria, Va., 2006.
18. Noålsund, R., E. Tutumluer, and I. Horvli. Degradation of Railway Ballast Through Large Scale Triaxial and Full Scale Rail Track Model Tests: Comparison with Mechanical Laboratory Tests. *Proc., 10th International Conference on Bearing Capacity of Roads, Railways and Airfields,* June 25–27, Trondheim, Norway, 2013.
19. Rao, C., E. Tutumluer, and I. T. Kim. Quantification of Coarse Aggregate Angularity Based on Image Analysis. In *Transportation Research Record: Journal of the Transportation Research Board, No. 1787,* Transportation Research Board of the National Academies, Washington, D.C., 2002, pp. 117–124.
20. Tutumluer, E., Y. Qian, Y. M. A. Hashash, J. Ghaboussi, and D. Davis. Discrete Element Modeling of Ballasted Track Deformation Behavior. *International Journal of Rail Transportation,* Vol. 1, Nos. 1–2, 2013, pp. 57–73.

21. Qian, Y., S. J. Lee, E. Tutumluer, Y. M. A. Hashash, D. Mishra, and J. Ghaboussi. Simulating Ballast Shear Strength from Large-Scale Triaxial Tests: Discrete Element Method. In *Transportation Research Record: Journal of the Transportation Research Board, No. 2374*, Transportation Research Board of the National Academies, Washington, D.C., 2013, pp. 126–135.
22. Tutumluer, E., H. Huang, Y. M. A. Hashash, and J. Ghaboussi. Aggregate Shape Effects on Ballast Tamping and Railroad Track Lateral Stability. *Proc., Annual Conference of the American Railway Engineering and Maintenance-of-Way Association*, Sept. 17–20, Louisville, Ky., 2006.
23. Tutumluer, E., H. Huang, Y. M. A. Hashash, and J. Ghaboussi. Discrete Element Modeling of Railroad Ballast Settlement. *Proc., Annual Conference of the American Railway Engineering and Maintenance-of-Way Association*, Sept. 9–12, Chicago, Ill., 2007.
24. Tutumluer, E., H. Huang, Y. M. A. Hashash, and J. Ghaboussi. AREMA Gradations Affecting Ballast Performance Using Discrete Element Modeling (DEM) Approach. *Proc., Annual Conference of the American Railway Engineering and Maintenance-of-Way Association*, Sept. 20–23, Chicago, Ill., 2009.
25. Tutumluer, E., H. Huang, Y. M. A. Hashash, and J. Ghaboussi. Laboratory Characterization of Coal Dust Fouled Ballast Behavior. *Proc., Annual Conference of the American Railway Engineering and Maintenance-of-Way Association*, Sept. 21–23, Salt Lake City, Utah, 2008.
26. Tutumluer, E., Y. Qian, Y. M. A. Hashash, J. Ghaboussi, and D. D. David. Field Validated Discrete Element Model for Railroad Ballast. *Proc., Annual Conference of the American Railway Engineering and Maintenance-of-Way Association*, Sept. 18–21, Minneapolis, Minn., 2011.
27. Boler, H., M. Wnek, and E. Tutumluer. Establishing Linkages Between Ballast Degradation and Imaging Based Aggregate Particle Shape, Texture and Angularity Indices. *Proc., 2nd International Conference on Transportation Geotechnics*, Sept. 10–12, Hokkaido, Japan, 2012.
28. Moaveni, M., S. Wang, J. M. Hart, E. Tutumluer, and N. Ahuja. Evaluation of Aggregate Size and Shape by Means of Segmentation Techniques and Aggregate Image Processing Algorithms. In *Transportation Research Record: Journal of the Transportation Research Board, No. 2335*, Transportation Research Board of the National Academies, Washington, D.C., 2013, pp. 50–59.

The opinions expressed in this paper are solely those of the authors and do not represent the opinions of the funding agency.

The Railway Maintenance Committee peer-reviewed this paper.